Available online at www.sciencedirect.com
ScienceDirect
International Journal of Heat and Mass Transfer 50 (2007) 942–948
International Journal of HEAT and MASS TRANSFER
www.elsevier.com/locate/ijhmt

Buoyancy-driven convection of water near its density maximum with partially active vertical walls

P. Kandaswamy *, S. Sivasankaran, N. Nithyadevi

UGC-DRS Centre for Fluid Dynamics, Department of Mathematics, Bharathiar University, Coimbatore 641 046, India

Received 31 December 2005; received in revised form 20 July 2006
Available online 23 October 2006

Abstract

Transient natural convection of cold water around its density maximum in a square cavity is studied numerically. Nine different positions of the active zones are considered. The governing equations are solved using Control volume method with power low scheme. The results obtained for various values of parameters are presented graphically in the form of streamlines and isotherms. It is found that the average Nusselt number behaves non-linearly as a function of Grashof number. The heat transfer rate is decreased in the density maximum regions.

Keywords: Transient convection; Partially active walls; Square cavity; Density maximum

1. Introduction

The buoyancy-driven convection in a fluid-filled cavity is a topic of interest for many researchers, due to its wide ranging of applications in cryogenic industry, cooling problems, crystal growth techniques, space applications, etc. Free convection arises in a fluid due to the density variations caused by the temperature differences of the system. In most of the analysis pertaining to the convection of water in enclosures, a linear temperature–density relationship was taken. But in practice this will never happen as the density of water varies with temperature in a nonlinear fashion, attaining its maximum density around 4 °C.

Ho and Tu [1] experimentally and numerically investigated the natural convection of water near its maximum density at high Rayleigh numbers. They observed oscillatory convection flow and temperature fields in the enclosure and provide a good agreement with the measured time period of the cyclic traveling wave motion of the maximum density contour. Kandaswamy and Kumar [2] studied the natural convection of water near its density maximum in the presence of uniform magnetic field. They observed that the effect of the magnetic field on the natural convection is to inhibit the heat transfer rate. The effect of density inversion on steady natural convection heat transfer of cold water is studied by Lin and Nansteel [3]. They found convection is reduced due to the density maximum.

Mahidjiba et al. [4] investigated onset of convection in a horizontal anisotropic porous layer saturated with water near 4 °C. It is found that the onset of motion dependent permeability ratio and inversion parameter. Michalek et al. [5] made a numerical benchmark study on natural convection for anomalous density variation of water, and compare performance of four different numerical methods. Convection in water above ice penetrates into the stably stratified region above the density maximum at 4 °C studied by Moore and Weiss [6]. They found steady convection occurs at Rayleigh numbers below the critical value predicted by linear theory. Pantokratoras [7] studied natural convection of water near the density extremum along a vertical plate with sinusoidal surface temperature variation. It is found that there is an inner boundary layer near the plate with periodic characteristics. Tong and Koster [10]

* Corresponding author. Tel.: +91 422 2426764; fax: +91 422 2422387.
E-mail address: pgkswamy@yahoo.co.in (P. Kandaswamy).

0017-9310/$ - see front matter © 2006 Elsevier Ltd. All rights reserved.
doi:10.1016/j.ijheatmasstransfer.2006.08.013

numerically studied transient natural convection of water layer near its density maximum. The results illustrated that the temperature difference which determines the position of the maximum density plane in the water layer, can alter flow field and heat transfer substantially.

Valencia and Frederick [11] studied natural convection of air in square cavity with half-active and half insulated vertical wall. Recently Sundaravadivelu and Kandaswamy [9] derived a nonlinear 4th degree polynomial approximation for the density–temperature relation. In this paper we study natural convection of water near its density maximum in a square cavity of partially heating vertical walls using the above said nonlinear density–temperature relation.

2. Mathematical formulation

Consider a two-dimensional square cavity of size L filled with water as shown in Fig. 1. A portion of the left wall is kept at a temperature θ_h and a portion of the right wall is at temperature θ_c, with $\theta_h > \theta_c$, $\theta_c = 0\,^{\circ}\mathrm{C} = 273\,\mathrm{K}$. The remaining portion of the cavity is insulated. Nine different cases will be studied here. That is, the hot region is located at the top, middle and bottom and the cold region is moving from bottom to top of their respective walls. The density of water behaves non-linearly as $\rho = \rho_0\left[1-\sum_{i=1}^{4}(-1)^i\beta_i(\theta-\theta_c)^i\right]$ with $\beta_1 = 6.8143\times10^{-5}$, $\beta_2 = 9.9901\times10^{-6}$, $\beta_3 = 2.7217\times10^{-7}$ and $\beta_4 = 6.7252\times10^{-9}$. A typical density plot is provided in Fig. 3. It is clearly seen from the figure our 4th order polynomial is agreed with universal data. Under these assumptions the equations governing the motion of a two-dimensional viscous incompressible fluid may be written in the vorticity–stream function formulation as

$$\frac{\partial\zeta}{\partial\tau}+U\frac{\partial\zeta}{\partial X}+V\frac{\partial\zeta}{\partial Y}=\nabla^2\zeta+\sum_{i=1}^{4}i(-1)^iGr_iT^{(i-1)}\frac{\partial T}{\partial Y} \tag{1}$$

$$\nabla^2\Psi=-\zeta \tag{2}$$

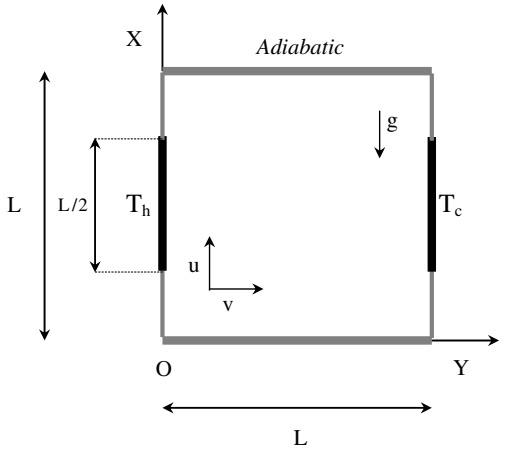

Fig. 1. Physical configuration.

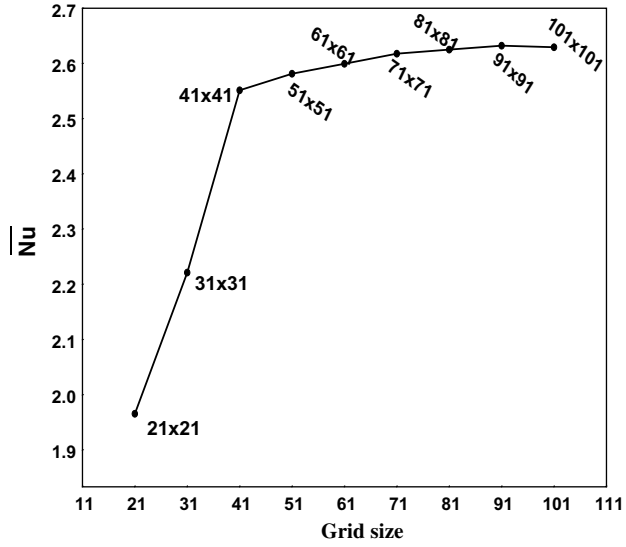

Fig. 2. Average Nusselt number versus different grid sizes for middle–middle heating location and $Gr_1 = 180{,}662$.

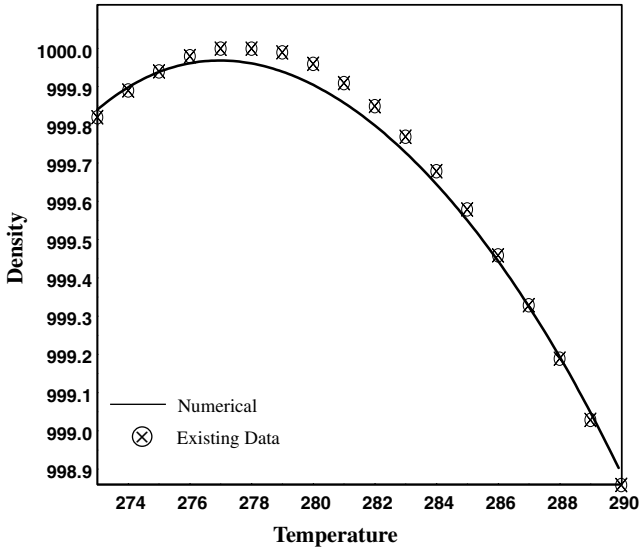

Fig. 3. Density versus temperature.

$$\frac{\partial T}{\partial\tau}+U\frac{\partial T}{\partial X}+V\frac{\partial T}{\partial Y}=\frac{1}{Pr}\nabla^2T \tag{3}$$

where

$$U=-\frac{\partial\Psi}{\partial Y},\quad V=\frac{\partial\Psi}{\partial X}\quad\text{and}\quad\zeta=\frac{\partial U}{\partial Y}-\frac{\partial V}{\partial X}. \tag{4}$$

The initial and boundary conditions in the dimensionless form are:

$\tau = 0;\ \Psi = 0 \quad T = 0$

$\tau > 0;\ \Psi = \frac{\partial\Psi}{\partial X} = 0 \quad \frac{\partial T}{\partial X} = 0$ at $X = 0$ and 1

$T = 1$ hot part, $T = 0$ cold part at $Y = 0$ and 1

$\frac{\partial T}{\partial n} = 0$ elsewhere at $Y = 0$ and 1

The nondimensional variables are $\tau = \frac{t}{L^2/\nu}, (X,Y) = \frac{(x,y)}{L}, (U,V) = \frac{(u,v)}{\nu/L}, \Psi = \frac{\psi}{\nu}, \zeta = \frac{\omega}{\nu/L^2}, T = \frac{\theta-\theta_c}{\theta_h-\theta_c}$.

The nondimensional parameters that appear in the equations are, $Gr_i = \frac{g\beta_i(\theta_h-\theta_c)^i L^3}{\nu^2}$ $i = 1,2,3,4$ Grashof numbers and $Pr = \frac{\nu}{\alpha} = 13.67$ Prandtl number, where g acceleration due to gravity, α thermal diffusivity, β coefficient of thermal expansion, ν kinematic viscosity, Ψ dimensionless stream function, τ dimensionless time, T dimensionless temperature, U and V dimensionless velocity components, X and Y dimensionless coordinates.

The local Nusselt number is defined by $Nu = \frac{\partial T}{\partial Y}\big|_{y=0}$ resulting in the average Nusselt number as $\overline{Nu} = \int_h Nu \mathrm{d}X$, where h is length of heating location.

3. Method of solution

The governing equations (1)–(4) were discretized using the finite volume formulation, with power law scheme, Patankar [8]. The region of interest was covered with m vertical and n horizontal uniformly spaced grid lines. The numerical solution was true-transient and fully implicit. At each time step the temperature and vorticity distributions were obtained from Eqs. (3) and (1) respectively. The streamfunction distribution was obtained from Eq. (2) by using successive over relaxation (SOR) and a known vorticity distribution. The dimensionless time step which yielded convergence for the majority of cases was $\tau = 10^{-4}$. An iterative process was employed to find the streamfunction, vorticity and temperature fields. The process was repeated until the following convergence criterion was satisfied,

$$\left|\frac{\phi_{n+1}(i,j) - \phi_n(i,j)}{\phi_{n+1}(i,j)}\right| \leqslant 10^{-5}. \quad (5)$$

The overall Nusselt number was also used to develop an understanding of what grid fineness is necessary for accurate numerical simulations. The numerical solution were done for different grid system from 21×21 to 101×101. After 41×41 grids, there is no considerable change in average Nusselt number, see Fig. 2. So 41×41 grid is used to find solutions for different parameters because of a grid containing 41×41 meshes yields satisfactory results.

4. Results and discussion

Numerical solutions for Grashof numbers provided in Table 1 that correspond to the cavity width 6 cm and hot wall temperatures between 277 K and 285 K are obtained and presented in the form of isotherms, streamlines and average Nusselt number. Fig. 4(a) and (b) illustrates the transient results of isotherms and streamlines for heating location top–bottom and $Gr_1 = 541{,}988$, $Gr_2 = 953{,}498$, $Gr_3 = 311{,}725$ and $Gr_4 = 92{,}431$. In the beginning, a small amount of fluid near the heating location is activated. A small anticlockwise vortex appears near the heating location. For $\tau = 0.01$, the isotherms are almost parallel lines.

Table 1
Calculated Grashof numbers for different hot wall temperatures

θ_h (K)	Gr_1	Gr_2	Gr_3	Gr_4
277	180,662	105,944	11,545	1141
281	361,325	423,777	92,362	18,257
282	406,491	536,342	131,509	29,245
283	451,657	662,151	180,396	44,575
285	541,988	953,498	311,725	92,431

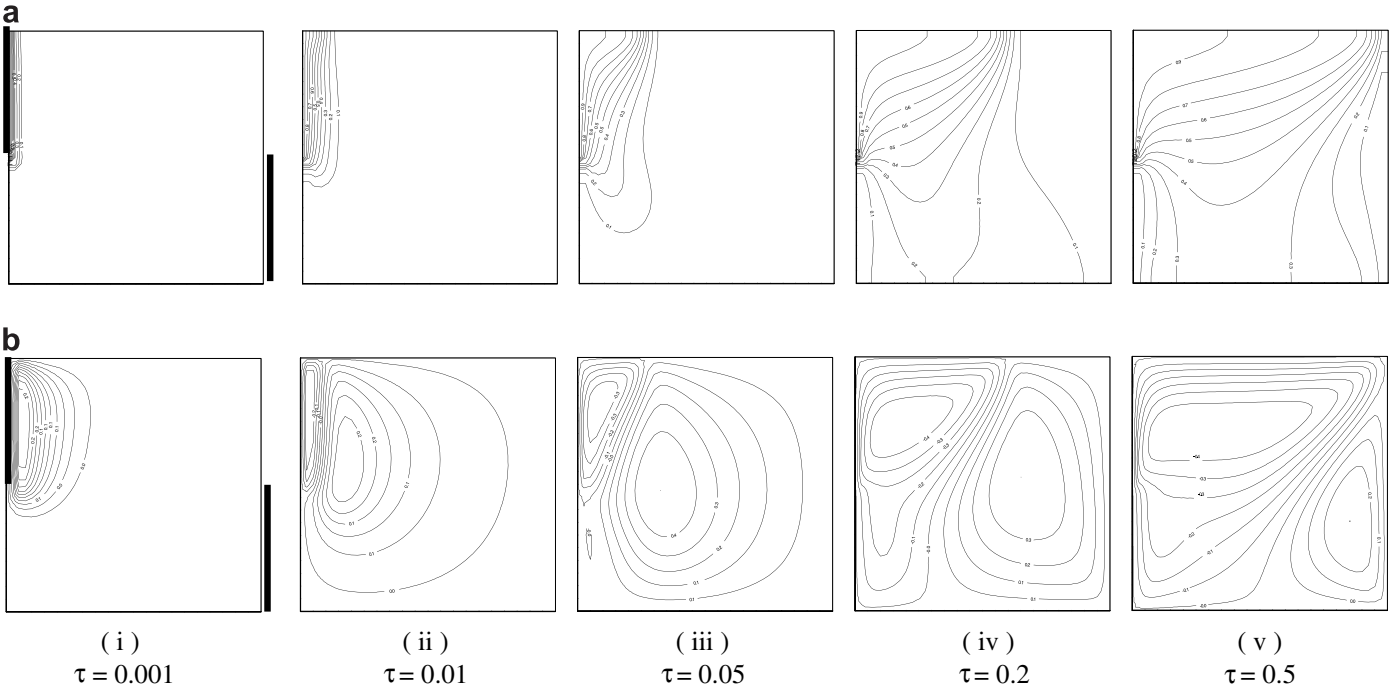

Fig. 4. (a) Unsteady state isotherms for top–bottom heating location and $Gr_1 = 541{,}988$. (b) Unsteady state streamlines for top–bottom heating location and $Gr_1 = 541{,}988$.

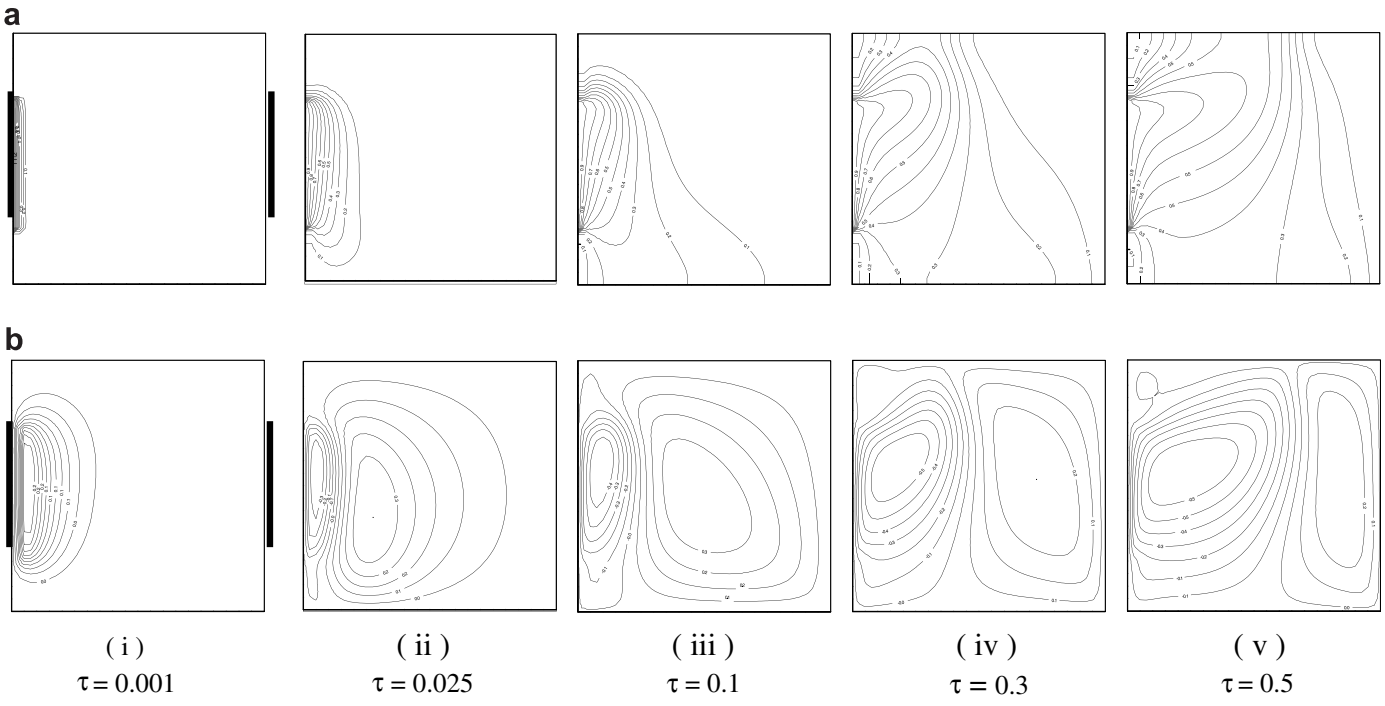

Fig. 5. (a) Unsteady state isotherms for middle–middle heating location and $Gr_1 = 541{,}988$. (b) Unsteady state streamlines for middle–middle heating location and $Gr_1 = 541{,}988$.

They indicate conduction mode of heat transfer. An existing small counter clockwise rotating vortex grows in its size and expands a bit away from heating location and then exists a small clockwise cell due to density inversion of water. At time $\tau = 0.05$, both vortex grows in its size. Further for increase in time $\tau = 0.2$ convection starts and buoyancy-driven flow throughout the enclosure is invigorated. At $\tau = 0.5$, it is evidently clear from the isotherms, the convection mode heat transfer dominates. The clockwise rotating cell grows, strengthens and suppresses its counterpart. Major portion of the cavity is occupied by clockwise rotating cell.

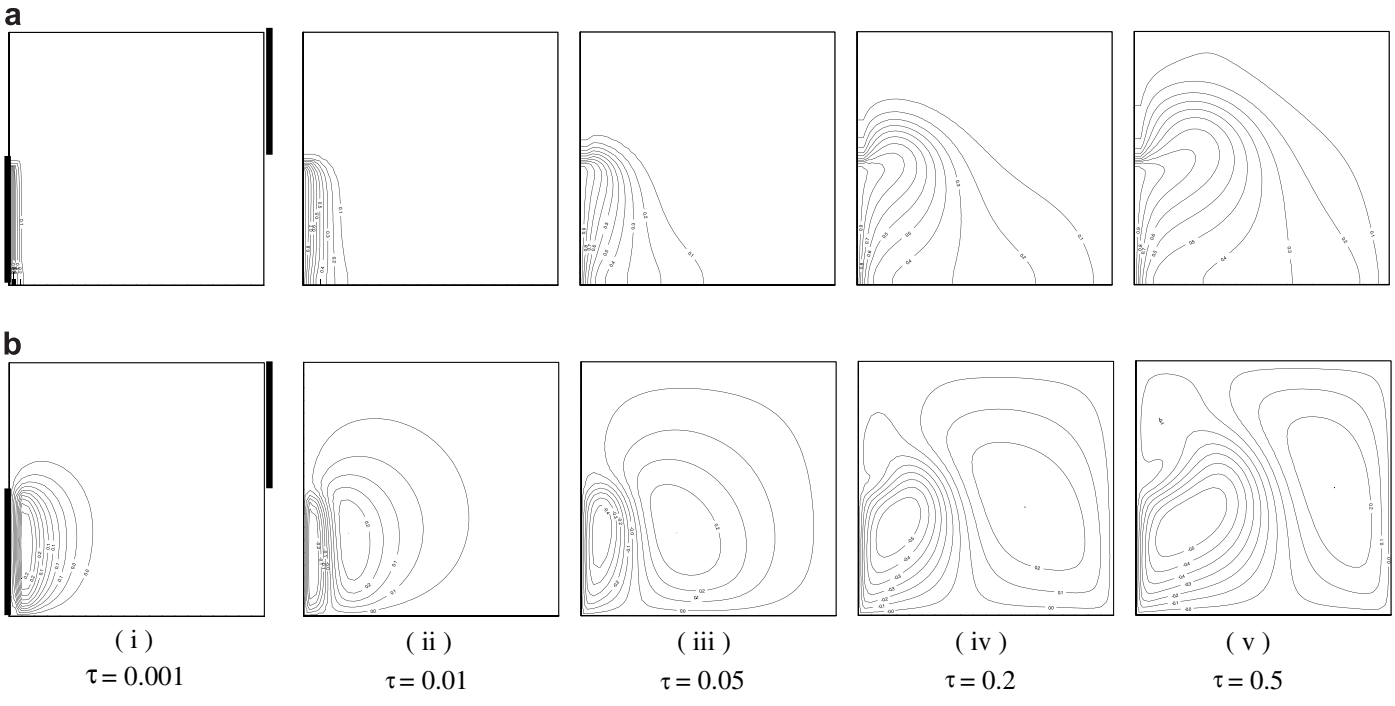

Fig. 6. (a) Unsteady state isotherms for bottom–top heating location and $Gr_1 = 541{,}988$. (b) Unsteady state streamlines for bottom–top heating location and $Gr_1 = 541{,}988$.

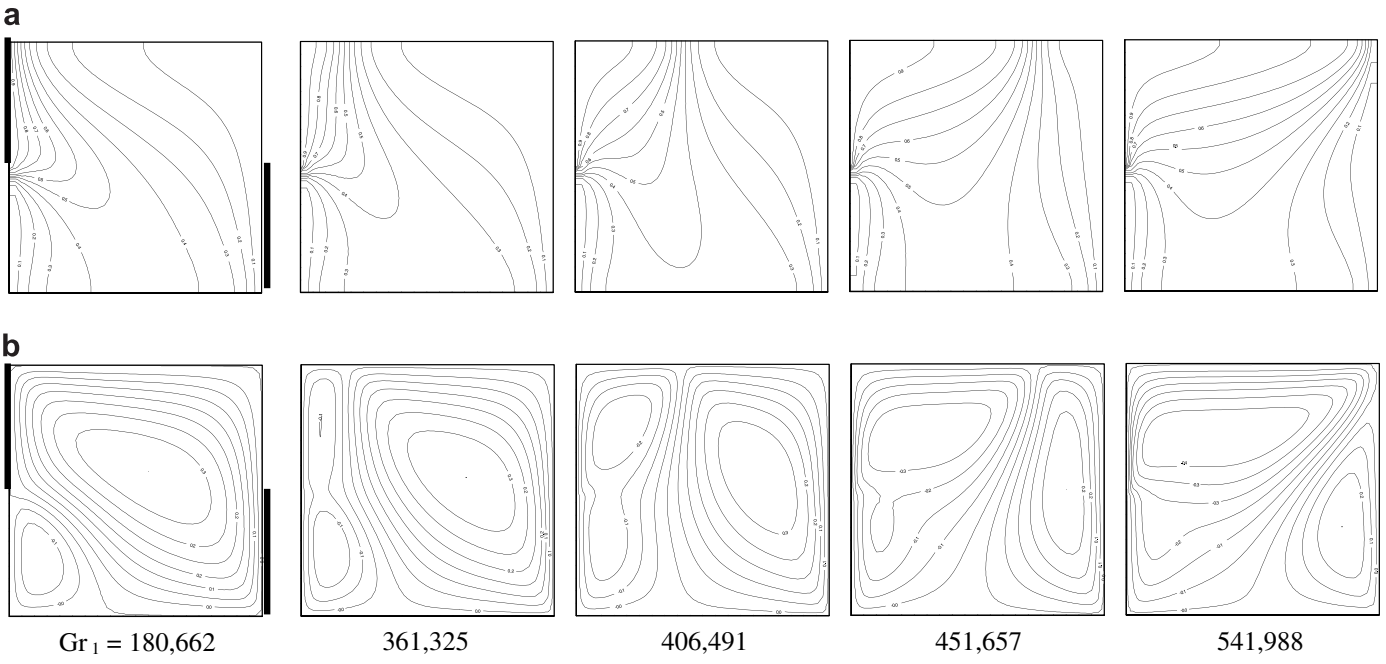

Fig. 7. (a) Steady state isotherms for top–bottom heating location. (b) Steady state streamlines for top–bottom heating location.

Transient results for different Grashof numbers and the middle–middle heating location are displayed in Figs. 5(a) and (b). At $\tau = 0.001$, one small buoyancy induced cell exists. Increasing the time, the cell moves towards the cold wall and one more buoyancy induced counter rotating cell exists near hot wall due to maximum density effects. Further increasing time, clockwise rotating vortex gains strength and anticlockwise vortex weakens. At $\tau = 0.3$ convection starts to dominate. The density of isotherms developing at the hot wall is higher than that at the cold wall. At $\tau = 0.5$, hot cell becomes large and cold cell shrinks its size because cells are separated by the $\Psi = 0$ plane at all times. The convective flow generated at the hot wall dominates the flow field all the time. The transient behaviour for different Grsahof numbers are displayed in Figs. 6(a) and (b). The same behaviour is observed as in the previous cases. The convection is weak due to infavorable buoyancy force because the heating location is at the bottom of the wall.

Figs. 7(a) and (b) show the heat and fluid flow pattern for different Grashof numbers. For $Gr_1 = 180{,}662$, 361,325, 406,491, 451,657 and 541,988 counter rotating eddies appear inside the cavity with one primary eddy circulating

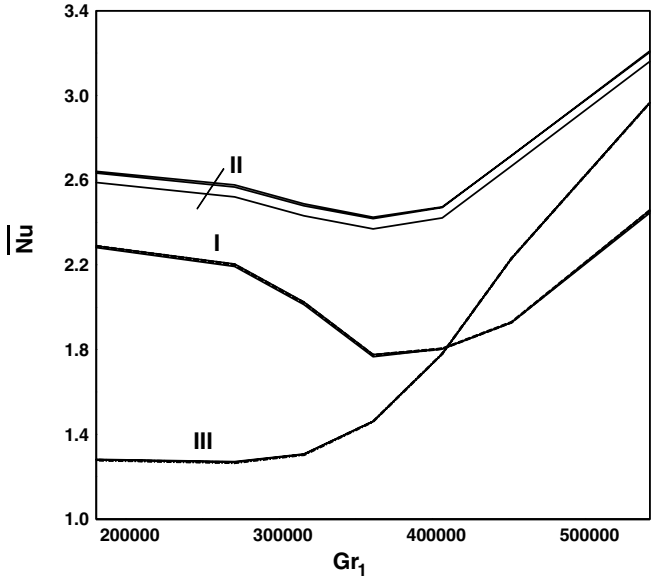

Fig. 8. Average Nusselt number versus Grashof number.

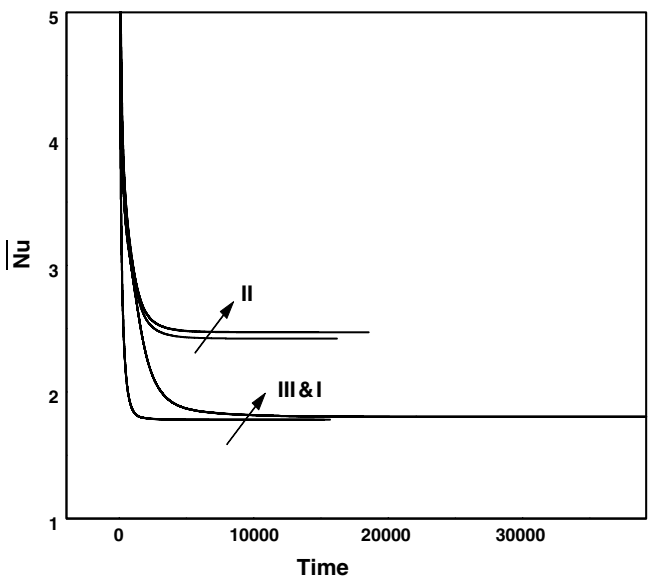

Fig. 9. Time history of average Nusselt number for $Gr_1 = 451{,}657$.

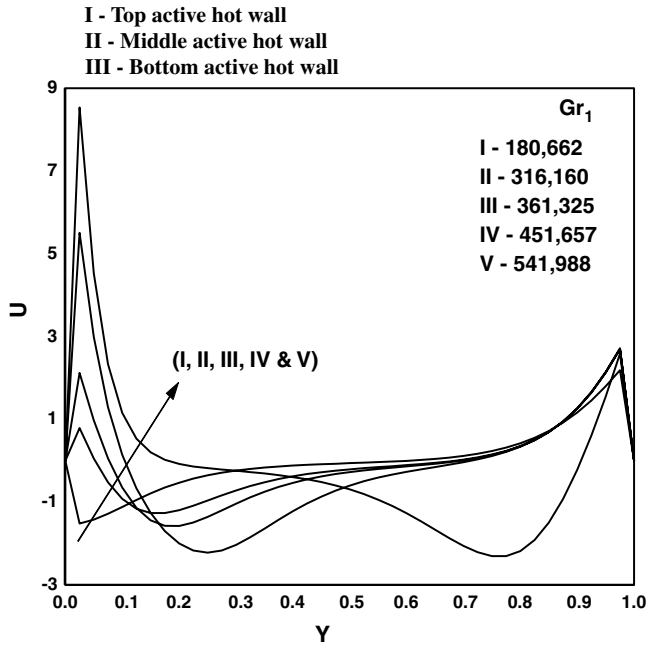

Fig. 10. Vertical velocity profiles at mid-height for middle–middle heating location.

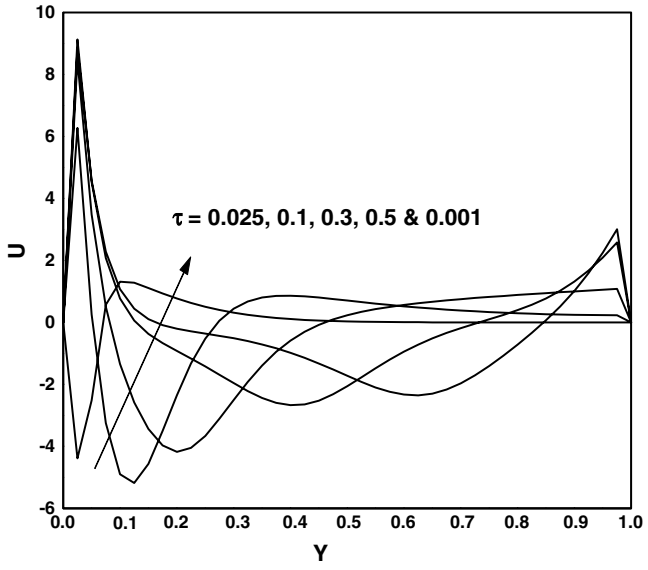

Fig. 12. Time dependent vertical velocity profile at $Gr_1 = 451{,}657$.

in counter clockwise direction near cold wall and secondary eddy near the hot wall below the heating location. Due to existence of counter rotating flow pattern, a transition from convection to conduction type of heat transport is observed. We observe that the hot wall vortices grow inside with increasing Grashof numbers by suppressing their respective cold wall vortices. Therefore the convection mode of heat transfer is dominated within the enclosure.

Fig. 8 shows the average Nusselt number for different heating locations. It is clearly seen from the figure the average Nusselt number behaves non-linearly as a function of Grashof numbers. At the density maximum region the heat transfer rate is reduced after that it is increased gradually. The heat transfer rate is enhanced when the heating location is at middle for all values of Grashof numbers. It is observed there is no considerable change in rate of heat transfer for change the position of cold wall while hot part is fixed. Fig. 9 shows the time history of the average Nusselt number for different Grashof numbers. As time evolves the particles near the hot wall have higher temperature and so the heat transfer rate starts decreasing then we get sudden fall in the values of average Nusselt number as seen to

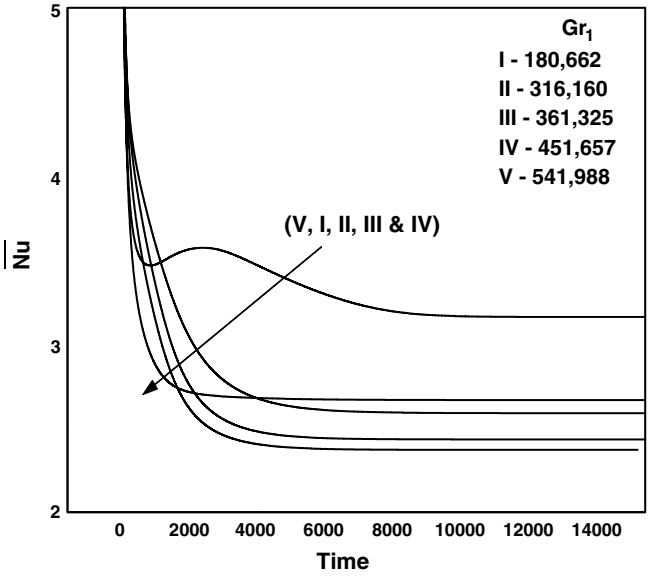

Fig. 11. Time history of average Nusselt number for middle–middle heating location.

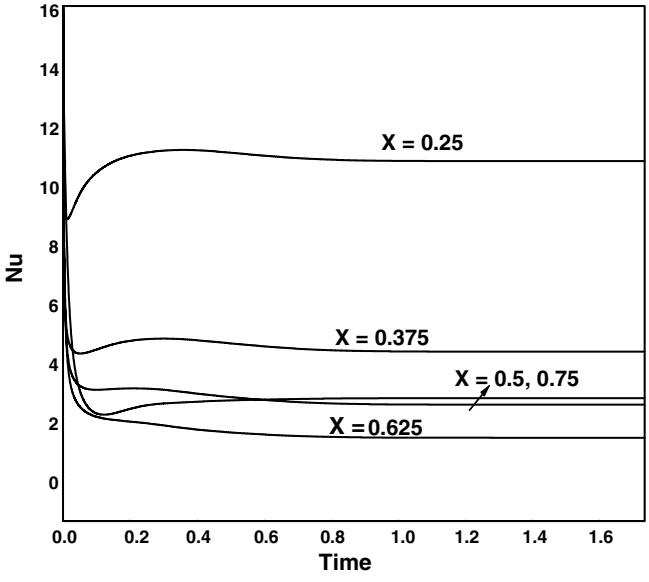

Fig. 13. Variation of the transient local Nusselt number with τ at $Gr_1 = 451{,}657$.

be constant. The middle hot wall heating gives the high heat transfer rate among all three locations.

Fig. 10 shows the mid-height velocity profile for different Grashof numbers and middle–middle heating location, the velocity reaches its peak near the hot wall and increases with Grashof numbers. To evaluate how the buoyancy affects the heat transfer along the hot wall, average Nusselt number is plotted as a function of Grashof number. First the rate of heat transfer is decreased and after density maximum it is increases with Grashof number. It is seen from Fig. 11 that the density inversion affects the natural convection and heat transfer. Fig. 12 shows the development of transient velocity profiles. The velocity of the particle near the heating location is increased with increasing time. The variation of the transient local Nusselt number with time τ along the hot wall of the cavity at different positions X is presented in Fig. 13. It is seen that immediately after the process of the local Nusselt number decreases for a short time and then reach the steady state value. For low values of X, the local Nusselt number attains the maximum value. Increase X, the local Nusselt number decreases upto a certain level and then increases for fixed value of Grashof numbers.

5. Conclusion

It is found that the heat transfer rate is enhanced when the heating location is at middle of the hot wall for all values of Grashof numbers. There is no considerable variation on natural convection on changing the active zones of the cold wall for fixed hot wall zones. The average Nusselt number behaves non-linearly as a function of Grashof number and heat transfer is reduced in the maximum density region. Increasing Grashof numbers decreases heat transfer up to density maximum and then increases.

References

[1] C.J. Ho, F.J. Tu, Visualization and prediction of natural convection of water near its density maximum in a tall rectangular enclosure at high Rayleigh numbers, J. Heat Transfer 123 (2001) 84–95.
[2] P. Kandaswamy, K. Kumar, Buoyancy-driven nonlinear convection in a square cavity in the presence of a magnetic field, Acta Mech. 136 (1999) 29–40.
[3] D.S. Lin, M.W. Nansteel, Natural convection heat transfer in a square enclosure containing water near its density maximum, Int. J. Heat Mass Transfer 30 (1987) 2319–2329.
[4] A. Mahidjiba, L. Robillard, P. Vasseur, On set of convection in a horizontal anisotropic, Int. Commun. Heat Mass Transfer 27 (2000) 765–774.
[5] T. Michalek, T.A. Kowalewski, B. Sarler, Natural convection for anomalous density variation of water: Numerical benchmark, Progr. Comput. Fluid Dyn. 5 (2005) 158–170.
[6] D.R. Moore, N.O. Weiss, Nonlinear penetrative convection, J. Fluid Mech. 61 (1973) 553–581.
[7] A. Pantokratoras, Laminar natural convection in water near the density extremum along a vertical plate with sinusoidal surface temperature variation, Acta Mech. 172 (2004) 211–218.
[8] S.V. Patankar, Numerical Heat Transfer and Fluid Flow, Hemisphere, McGraw-Hill, Washington, DC, 1980.
[9] K. Sundaravadivelu, P. Kandaswamy, Combined buoyancy and thermocapillary convection of cold water around its density maximum temperature, Acta Mech. 147 (2001) 209–218.
[10] W. Tong, J.N. Koster, Density inversion effect on transient natural convection in a rectangular enclosure, Int. J. Heat Mass Transfer 37 (1994) 927–938.
[11] A. Valencia, R.L. Frederick, Heat transfer in square cavities with partially active vertical walls, Int. J. Heat Mass Transfer 32 (1989) 1567–1574.